A Surprising Boost in Starlink Satellite Brightness at Optical Wavelengths During the Day

Sarah Elizabeth Caddy
Australian Astronomical Optics, Macquarie University, Sydney, Australia
School of Mathematical and Physical Sciences, Macquarie University, Sydney, Australia
Lee Robert Spitler
Australian Astronomical Optics, Macquarie University, Sydney, Australia
Astrophysics and Space Technologies Research Centre, Macquarie University, Sydney, Australia

ABSTRACT

The rapid increase in satellite launches in recent years, and the pressure of launches planned into the next decade, demands an improvement in the efficiency of space domain awareness facilities. Optical facilities form an important component of global space domain awareness capabilities, however traditional optical telescopes are restricted to observing satellites during the relatively short twilight periods. In this work we explore expanding this operational period to encompass the entire day to dramatically improve the observing opportunities at a single site. We explore daytime space domain awareness observations with the Huntsman Telescope Pathfinder, an instrument built using predominantly off the self components, and a Canon telephoto lens. We report photometric light curves of 81 Starlink satellites from Sun altitudes ranging 20 degrees to midday. Starlink satellites are found to be particularly bright at 3.6 ± 0.05mag, $\sigma = 0.6 \pm 0.05$mag in sloan r', or $\sim 11\times$ brighter than twilight conditions. After a comparison to a theoretical model, we conclude this surprising observed brightness is due to the contribution of Earthshine beneath the orbiting satellites. Finally we discuss the potential for the Huntsman Telescope Pathfinder to use daytime light curves to detect changes in the orbiting orientation of satellites.

1. INTRODUCTION

The largest single contributor to recent Low Earth Orbit (LEO) satellite launches, are Starlink satellites. Starlink is currently the worlds largest satellite constellation[1] and - as of April 2024 make up over half of all active satellites[2] in LEO. With planned LEO launches into the future only increasing in the era of mega constellations, we must improve our capabilities to monitor space assets to ensure a safe environment for all satellite operators[3, 37, 38].

Twilight optical Space Domain Awareness (SDA) facilities have become a cornerstone of global SDA capabilities widely used by both governments and multi-national collaborations, to individuals and private industry [22]. This has been driven in part by the rise of commercial off the shelf technologies (COTS) driving down prices and development times for optical facilities [22], and where global radar facilities have not yet been favoured due to the trade off between cost and performance [22].

Optical SDA observations however, have limitations. Historically, optical observations of LEO satellites from the ground have been restricted to terminator illuminated conditions [39, 12, 29] or "twilight". This is a configuration where the observer is in the Earth's shadow just after Sunset, and the satellite is illuminated by the Sun. Further restrictions arise where LEO satellites pass into the Earth's shadow and become too faint for an optical SDA facility to detect them via reflected Sunlight [12]. In addition, when restricted to twilight, some satellites may only be visible for a few minutes - if at all - every few weeks from a given observing location [40]. For example, using a sample of 755 Starlink V1.5 satellites[3] observable in a typical 24 hour period in summer at Macquarie University Observatory in Sydney, Australia, we estimate 74% of observable passes occur during the day, and only 26% are twilight illuminated passes.

[1] https://www.starlink.com/au/technology
[2] https://www.keeptrack.space/deep-dive/starlink-vs-the-world/
[3] https://github.com/Forrest-Fankhauser/satellite-optical-brightness/blob/main/data/brightness_config_list.csv

If SDA facilities could operate effectively all day instead of just during twilight conditions, this would greatly improve the productivity of global optical SDA facilities. Daytime observation would allow us to take advantage of all Sunlit passes of satellites above an observing location (both during twilight and during the day). More frequent observations of satellites combined with GPS timing enabled by daytime observations will ultimately result in a decrease in the uncertainty of satellite orbital elements, and an accurate orbital determination [12].

In addition to a single detection of a satellite in LEO during the day, tracking and producing accurate photometric light curves provides another dimension of information that is useful for SDA analysis. Many studies conducted have demonstrated the importance of light curves as an essential tool for characterising and classifying LEO satellites during twilight and Geostationary Orbit (GEO) satellites at night based on their material properties, as well as capturing both position and dynamics information [27, 23, 5, 26, 20, 21, 18, 10, 35, 34, 33, 4, 25].

Light curves of LEO and GEO satellites have also been studied during twilight and night respectively to determine their rotation about their center of mass, particularly for satellites that are tumbling out of control [21, 34, 33, 4, 25]. Almost all of these satellites in LEO and GEO are too small to directly resolve, and so light curves remain the most effective way of monitoring the rotational period. Satellites without active stabilisation begin to tumble under the influence of forces that are poorly understood which in combination with flat reflective surfaces on the body of the satellite produces periodic glints which can be used to determine rotational velocity [10, 24, 2].

Daytime observations are expected to be boosted in brightness by Earthshine, following the results of Fankhauser et al. (2023) [13] in twilight conditions. Earthshine consists of two components: 1) re-radiated infrared light and 2) scattered Sunlight. At $\sim$ 0.3-2μm Earthshine is dominated by reflected Sunlight and predominantly bluer in colour [8]. Earthshine has been shown through simulations and comparison to data in twilight terminator illuminated conditions to contribute to satellite optical brightness in LEO [13]. In addition, in conditions where Earthshine is brightest, typically where there is ice or large systems of clouds below the satellite in LEO, [39] predicts that satellites may be illuminated comparably to terminator illuminated conditions.

Optical daytime observations however, are challenging. The bright sky background and increased atmospheric turbulence due to large temperature gradients during the day result in low signal-to-noise (SNR) detections, and bright detection limits [9, 40, 32, 19, 39, 12]. For optical daytime observations to be successful, a well calibrated robotic telescope mount is required, equipped with photometric broadband filters to reduce the bright sky background [9]. Further, recent improvements in Complimentary Metal Oxide Semiconductor (CMOS) detectors has resulted in cameras that now rival the quality of Charged Couple Device (CCD) detectors [1]. They have enabled the high frame rate observations required to take multiple rapid observations of a moving target, preventing over exposure and enabling stacking of data to achieve higher SNR detections [9].

So far, detecting a LEO satellite during the day has been successfully attempted by a number of groups [40, 32, 12, 30, 9, 31]. These investigations span the optical and near infrared, and most were motivated by the need to 'close the daylight gap' [12] and build cathermal SDA facilities that operate both during twilight, night (for GEO) and during the day [e.g., 32, 31]. Notably, Zimmer et al. (2021) [40] reports single detections of Starlink satellites up to magnitudes as bright as 2.6 in visual wavelengths, but were unable to explain the reason for this surprising increase in brightness.

In this work, we demonstrate the successful detection, collection and characterisation of Starlink light curves during the day, at a range of Sun altitudes, including midday. For this work we use an optical SDA facility, The Huntsman Telescope Pathfinder [9], which is a test facility located at Macquarie University, Sydney Australia. It is designed to test experimental science cases for the Huntsman Telescope, a robotic $<$0.5 m class research facility located at Siding Spring Observatory, Australia on Gamilarray, Wiradjuri and Wayilwan country [17]. While the Huntsman Telescope was originally designed for low surface brightness imaging at night, its high étendu, large field of view and good stray light control are properties that are ideal for daytime SDA.

In the work of Caddy et al. (2024) [9] we show that the Huntsman Telescope Pathfinder is capable of 1-10% photometry during the day, so extending this work to capturing light curves of satellites is a natural next step. We detail our observing methods, and present light curves for 81 Starlink satellites spanning version V1.0 to V2.0, and explore the factors influencing the brightness of satellites during the day, and the implications of this work in the era of satellite mega constellations.

Fig. 1: Left, The Huntsman Telescope Pathfinder consisting of a single Canon lens used in this work. The Rowe-Ackermann Schmidt Astrograph our setup is attached to is not used in this work. The unit is located at Macquarie University Observatory, Sydney, Australia. Right, The Huntsman Telescope facility located at Siding Spring Observatory, Australia. Both telescopes use Canon 400 mm f/2.8 lenses with a pixel scale of 1.24'. The 10 lenses are configured to cover the same field of view of $1.89^\circ \times 1.26^\circ$.

2. METHOD

Observations are conducted over January to March of 2024 using the Huntsman Telescope Pathfinder at Macquarie University Observatory, Sydney, Australia. This instrument is identical to the Huntsman Telescope, except it comprises of only one Canon lens, as opposed to an array of 10. We use a single Canon 400mm f/2.8 lenses with a field of view (FOV) of $1.89^\circ \times 1.26^\circ$ and a pixel scale of 1.24". Following the results of Caddy et al. (2024), the lens has a filterwheel containing a sloan r' filter which we use for this work in order to minimise the sky brightness during the day. We use an Astromechanics focuser[4], and a ZWO ASI183MM Pro[5] camera and a Software Bisque Paramount MEII mount [6].

2.1 Photometry

Photometric calibration flat field data are taken at twilight after each observing session. Flats are taken during twilight to reduce the prominence of the sky gradient in the flats taken during the day [9]. We do not use darks or bises in this work. Approximately 100 sloan r' flats are median combined to create a master flat that is used to calibrate the science frames. Following the results of Caddy et al. (2024)[9], to perform aperture photometry, we use a fixed aperture radius of 11 pixels for all images to maximise the target flux in the aperture over a range of seeing conditions (our targets range from $\sim$ 3 to 6 arcseconds FWHM typically). This overly generous aperture reduces impact from variable seeing,

[4]https://astromechanics.org/
[5]https://astronomy-imaging-camera.com/product/asi183mm-pro-mono/
[6]https://www.bisque.com/product/paramount-me-6/

which otherwise would require variable aperture corrections to be applied. The calibrated apparent magnitude is then:

$$r' = r'_{inst} - ZP_{r'} - k_{r'}(X)$$

Where r'_{inst} is the instrument magnitude in units of e^-/s, r' is the calibrated magnitude, $ZP_{r'}$ is the system zeropoint, $k_{r'}$ is atmospheric extinction coefficients, and X is the airmass at the time of the measurement. As we do not have multi-wavelength observations of our targets, we do not perform a colour correction.

A detailed exploration of the Huntsman Pathfinder's photometric accuracy during the day can be found in [9]. For sloan r' we adopt the measurements of [9] of $ZP_{r'} = -21.7$ and $k_{r'} = 0.34$. The total photometric accuracy is reported to be a median of 0.05 mag in Sloan r' with a standard deviation of 0.03 mag throughout the duration of the 7 month campaign described in [9]. In this work we do not take separate reference star calibration observations, and instead use the median zeropoint, extinction coefficient, and colour coefficient over the [9] work.

During processing, for each target observation the TLE is retrieved by special data request in Celestrak for the time and date when an image is taken. The TLE, observatory site location details and timestamps for each frame are input into the `skyfield` [28] EarthSatellite and Topos class instances, and this is used to derive the satellite altitude in meters at the time of observation, the longitude and latitude of point on the surface of the Earth directly below the satellite and the satellite altitude and azimuth from the observers location at the time of observation. `Astropy` [36] is used to compute the Sun coordinates with respect to the observer, from which we calculate the angular separation of the target from the Sun on sky.

2.2 Satellite Optical Brightness Modelling

We compare our observations against a satellite optical brightness model called `lumos-sat`[7] described in [13]. The software was not designed to produce daytime estimates of satellite brightness, and so minor alterations are made to remove exceptions thrown when the Sun altitude of an observation is above 0 degrees. The geometry of the problem implemented in `lumos-sat` remains the same and is not changed. The code models satellites as a collection of opaque surfaces, with a Bidirectional Reflectance Distribution Function (BRDF) [15] describing the angular distribution of light reflected from surface and takes the general form:

$$BRDF = f_r(\hat{w}_i, \hat{w}_o) \equiv \frac{1}{cos(\phi_o)cos(\phi_i)L_i}\frac{\partial L_o}{\partial \hat{w}_i}$$

Where L_i is the ingoing radiance and L_o is the outgoing radiance. ϕ_i is the angle between the surface normal and the vector to the source $\hat{w}_i$, and similarly $\hat{w}_o$ is the angle from the surface normal to the observer. The BRDF function describes the ratio of the spatially distributed, reflected radiance outgoing from a surface, to the incident irradiance. For example a shiny metallic surface or body of water may exhibit specular reflections at particular angles, compared to diffusely reflected light from a forest canopy, sandy beach, or coarse material on a satellite body. We consider two BRDF's in this work, as described in [13]. The Phong model is utilised to represent light scattered from the surface of the Earth and combines a lambertian BRDF where light is scattered equally or diffusely in all directions ($\frac{K_d}{\pi}$) with a specular peak component defined by:

$$BRDF = \frac{K_d}{\pi} + K_s\frac{n+2}{2\pi}(\hat{w}_r \cdot \hat{w}_o)^n$$

Where the K_d parameter controls of the magnitude of the diffuse component, K_s the magnitude of the specular component, and n controlling the width of the specular peak. $\hat{w}_r$ and $\hat{w}_o$ are the reflected and outgoing unit vectors respectively. Based on the recommendations of [13] a more complex Binomial BRDF model is used for satellite surfaces. The model is fit to data provided by SpaceX which was gathered in a lab specifically for the V1.5 satellite and is derived in [13] and implemented in `lumos-sat`.

For this work, we focus on Starlink satellites. Starlink satellites are largely comprised of two surfaces; the Solar panel and the chassis. We assume a nominal operating attitude described in [13] where the chassis points directly nadir, and

[7] https://github.com/Forrest-Fankhauser/lumos-sat

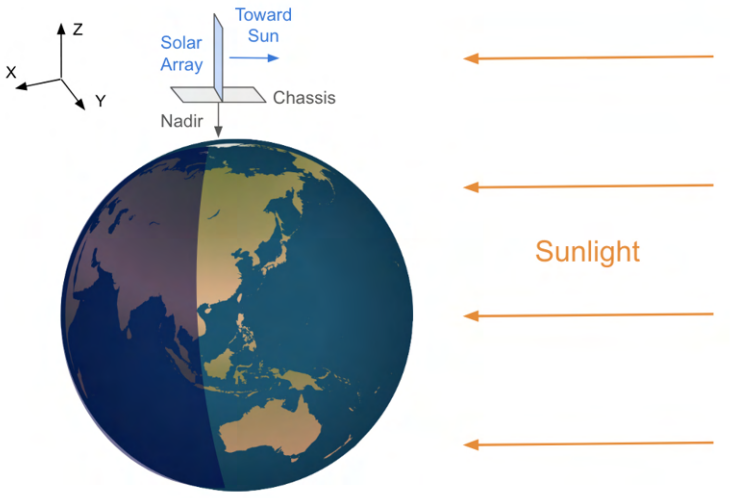

Fig. 2: Geometry of a Starlink satellite in orbit during midday, and in terminator illuminated conditions. In nominal operations, the chassis of the satellite points nadir, and the Solar panel at 90 degrees from the chassis.

the Solar panel is positioned perpendicularly to the chassis, and facing the direction of the Sun shown in Figure 2. This is known as the 'on station' configuration when the satellite has reached it's optimal altitude.

We categorise Starlink satellites by their version number and for this study target V1.0, V1.5 and V2.0 satellites. V1.5 Satellites are used in [13], and we use the surface areas of $3.65m^2$ for the chassis and $22.00m^2$ for the Solar array described in this work. Finding accurate estimates for V2.0 and V1.0 are more challenging due to the limited information SpaceX makes public about Starlink design. In a letter sent to the secretary of the federal communications commission [8], Starlink detail surface areas for versions of the V2.0 satellites, 2 of which are to be launched from the Falcon 9 launch vehicle that are now in orbit. These are the V2.0 with Solar array surface area of $22.68m^2$ and chassis of $3.64m^2$ similarly to the V1.5 satellites, and a larger "V2.0 mini" with Solar array surface area of $104.96m^2$ and chassis of $11.07m^2$. The larger of the two hosting two Solar panel arrays [9] with some being designated by the classification code C as opposed to U in the NORAD ID indicating their use for military purposes.

V1.0 satellites have even less publicly available information, however rough estimates[10] place the V1.0 at 4 times smaller than the V2.0 mini, similar to the V1.5. We use these estimates to form our model in `lumos-sat`. Due to the uncertainty around the design[11] and attitude at which the V1.0 and V2.0 satellites orbit, we exclusively use the V1.5 BRDF fitted using lab data from [13] to describe the scattering properties of the V2.0 mini and V1.0 satellites.

In order to compare our sloan r' band results with the model predicted brightness, we take an ASTM E-490 Solar spectrum and integrate it with the throughput of the sloan r' bandpass to determine a top of the atmosphere modified Solar constant of $1233W/m^2$. Neither `lumos-sat` or this work take into account atmospheric absorption and is out of the scope of this study.

3. RESULTS

3.1 Observed Satellite

We find that Starlink satellites are visible during the day using the Huntsman Telescope Pathfinder system. Of the 140 Starlink satellite passes we attempt to observe only 26% are non-detections either due to a technical fault or a non-visual detection in the region of the sky in which the satellite is targeted, leading to a success rate of 74%. This rate

[8] https://planet4589.org/astro/starsim/papers/StarGen2.pdf
[9] https://www.spacex.com/starshield/
[10] https://skyandtelescope.org/astronomy-news/the-newest-and-largest-starlink-satellites-are-also-the-faintest/
[11] https://circleid.com/posts/20230104-spacex-launches-second-generation-starlink-satellites

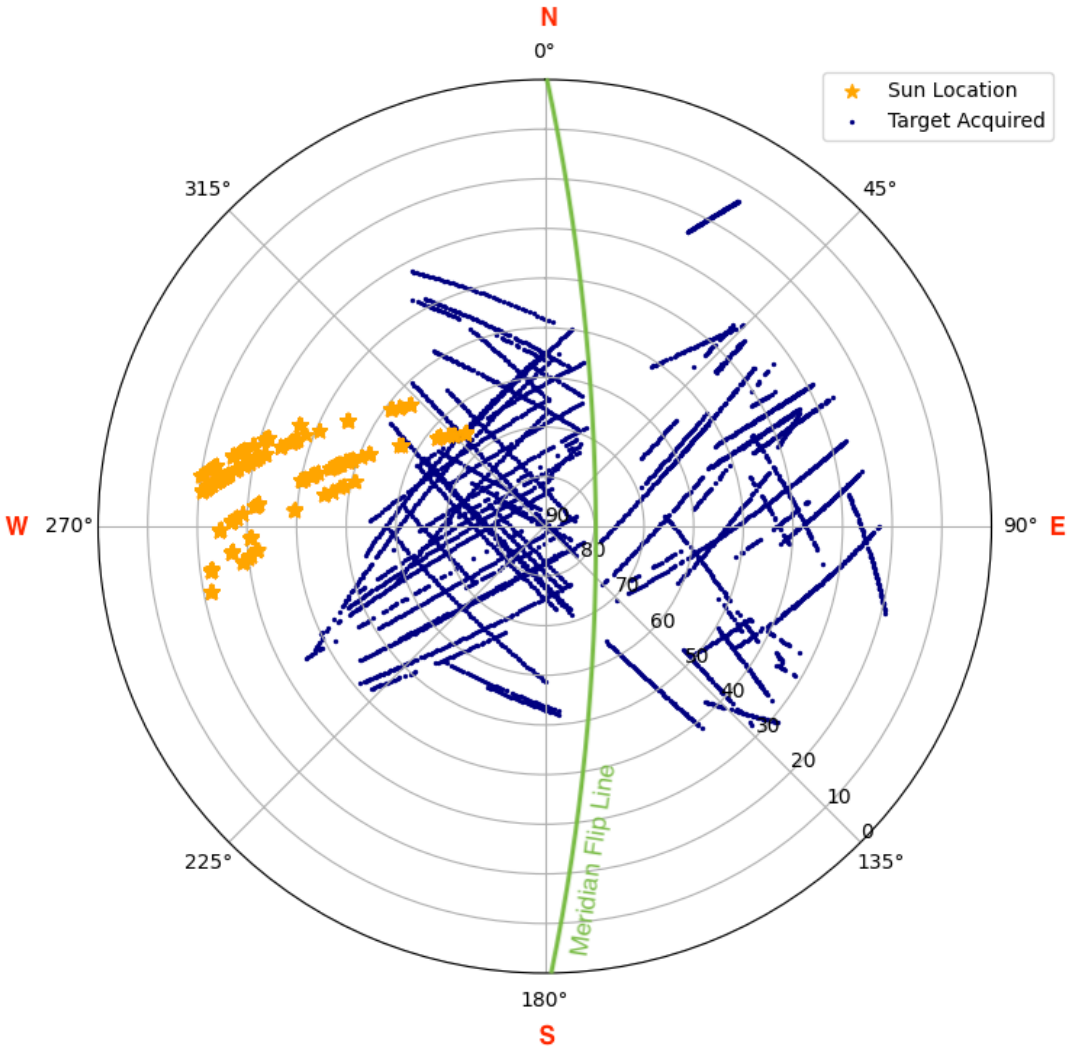

Fig. 3: The altitude and azimuth of all successful observations of satellites used for photometric analysis. The location of the Sun during these observations is also plotted for reference in yellow. Note the approximately 30 degree minimum altitude limit in the West due to obstructions from trees. A clear division between two groups of data in the West and East can also be seen due to the limitations of an equatorial mount. We allow a liberal 10 degrees max beyond zenith for this limitation (in the direction of travel), which is shown in green as the meridian flip line, in order to collect as much data as possible in this critical location of the pass.

increased to a maximum detection rate of 90% once the process of scheduling observations are optimised. To ensure precise photometry, we rigorously filter out any data showing visual signs of high cloud cover or bushfire smoke, regardless of whether a detection has occurred. Due to back burning that took place near our observing site during one of our observing runs, this left a sample size of 81 Starlink satellites passes that can be used for photometric analysis.

Successful observations span Sun altitudes from 65 degrees (summer, midday, at Australian latitudes) to 20 degrees. The angle between the target and the Sun on sky spans 133 degrees to 25 degrees. We achieve 1447 individual observations of 28 unique V2.0 satellites, 1598 observations of 35 V1.5 satellites, and 782 observations of 18 V1.0 satellites. At our observing site at Macquarie Observatory, observations are limited in the West due to obstructions by trees to an altitude of approximately > 30 degrees. In Figure 3 we present the altitude and azimuth of all of the observations made during this work that are used in photometric analysis, as well as the altitude and azimuth of the Sun at the time of observation. This plot highlights the limitations of an equatorial mount, which is the need for a

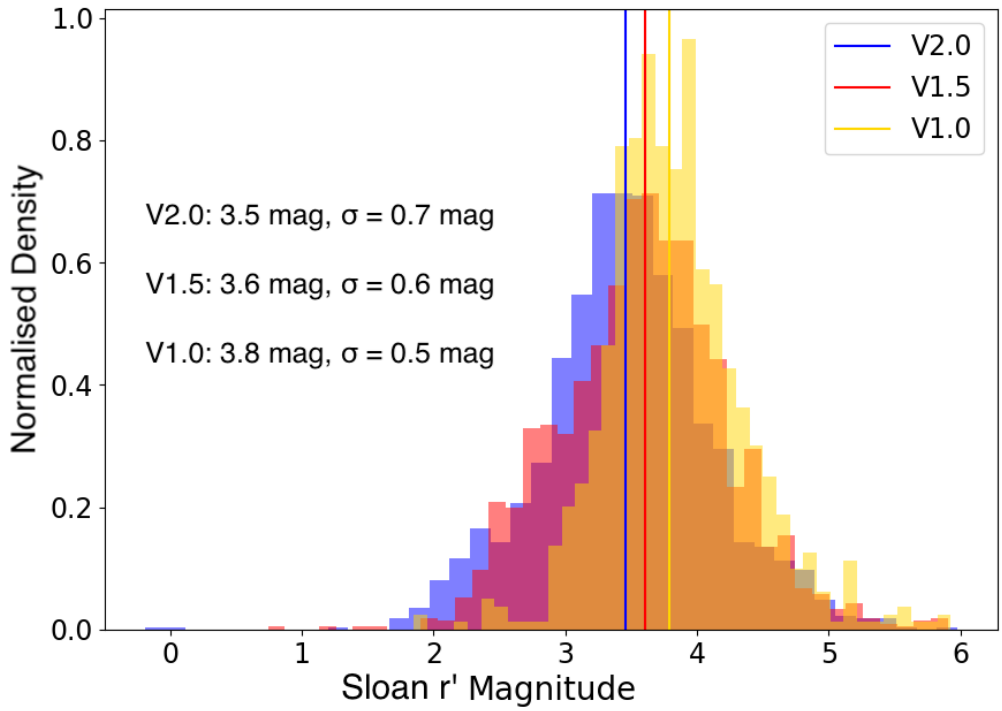

Fig. 4: The sloan r' magnitude of Starlink satellites observed during this survey. We include individual measurements from every exposure, and organise the data by satellite version. Considering all satellites, the median daytime r' magnitude is 3.6mag, $\sigma = 0.6$mag. For each satellite version, we find that the median magnitude increases from 3.8mag, $\sigma = 0.5$mag for V1.0, to 3.6mag, $\sigma = 0.6$mag for V1.5 and 3.5mag, $\sigma = 0.7$mag for V2.0. We also find that the standard deviation of this distribution increases for later models as well, indicating that the V2.0 satellites are on average brighter, and more significant variations in brightness over the duration of a pass. We note that there may be selection bias on the right hand side of the distribution due to our daytime detection limit, which is the most restrictive at V band 4.6 AB mag [9] for the highest sky surface brightness at midday.

meridian flip. As the telescope tracks East to West, to prevent the optical tube assembly from making contact with the pier the instrument must stop, turn 180 degrees and recommence tracking. Due to the time that this takes, only half of every pass is captured.

The 10-20 degrees delays in acquisition from the meridian is a result of the acquisition time for the mount to settle on the object once the tracking command is sent, and takes up a much larger angular area on sky than the Western pass due to the fact the object is travelling fastest near zenith. We should note that there is also observer bias as to which satellites and passes are chosen. Passes chosen opportunistically, not predetermined, and are chosen to reduce travel time between targets, minimise the strain on the mount (few meridian flips), and maximise the time on sky observing.

3.2 Satellite Optical Brightness During the Day

We find a median observed daytime magnitude for Starlink satellites of 3.6 ± 0.05mag, $\sigma = 0.6 \pm 0.05$mag, where 0.05mag is calculated the photometric error. This remains the same for all observations, so we do not report the photometric error for every detection. Examining the distribution of observations for each satellite version, we find that the median magnitude increases from 3.8mag, $\sigma = 0.5$mag for V1.0, to 3.6mag, $\sigma = 0.6$mag for V1.5 and 3.5mag, $\sigma = 0.7$mag for V2.0. The standard deviation of the distributions for each satellite version increases with later versions, indicating that they may undertake more significant variations in brightness over the duration of a pass.

Compared to twilight observations of Pomenis observatory data in [13], on average Starlink satellites are $\sim 11\times$ brighter during the day than at twilight, and as much as $\sim 14\times$ brighter at larger Solar phase angles. This unexpected

boost in brightness means that the Huntsman Telescope Pathfinder, a modest, low-cost visible wavelength telescope has been demonstrated to detect 90% (see section subsection 3.1) of Starlink satellites that pass overhead during the day. The typical magnitude we find are higher than the median measured brightness of satellites taken at twilight conditions at Pomenis observatory of ~ 2.6mag, and a smaller standard deviation of 0.6mag as compared to the ~ 1.0mag in Pomenis data.

3.3 Satellite Light Curves

To determine if information about each satellite for the purposes of classification and attitude determination can be gathered from photometric light curves, we plot all observations as a function of Solar phase angle shown in Figure 5. Larger Solar phase angles indicate a target that is close to the Sun on sky, and small Solar phase angles are targets that are far away from the Sun on sky. We also plot the twilight observations of V1.5 satellites from the work of [13] using data from the Pomenis observatory. Solar phase angle regions are labeled as "Solar array backscatter", "diffuse chassis scatter" and "specular chassis scatter" regions

Our data support the conclusion of [13] that Starlink satellites have a complicated relationship with Solar phase angle and are not well-represented by a cubic fit, which worked well for the Pomenis twilight data of only V1.5 Starlink satellites [13]. The growing complexity of light curves with each generation of Starlink satellite may be explained by the growing complexity of the design and operation of the satellites with each new version which is further explored in subsection 3.4. We also notice a lack of V1.5 and V1.0 satellites at Solar phase angles greater than ~ 60 degrees. This may be a selection bias due to our small dataset, or it could be due to a bias imposed by the daytime detection limit of the Huntsman Telescope Pathfinder as a function of sky brightness [9] due to the apparent decrease in brightness at smaller phase angles for these satellite versions. Solar phase angles greater than ~ 60 degrees is also where light is dominated by Solar array back-scatter [13], and so may be brighter and thus more likely to be detected against the bright daytime sky background for V2.0 satellites with two large Solar panel arrays surface area as compared to V1.0 and V1.5. as described in [13].

3.4 Differences Between Starlink Versions

We now consider individual light curves for each observed target as a function of Solar phase angle in Figure 6. Data is organised by satellite version, and 7 data points are rolling medians over time to reduce seeing/scintillation noise due to atmospheric turbulence that is significant during the day [9].

In Figure 6 the V1.0 satellites show a roughly linear trend with Solar phase angle from $\sim 80 - 140$ degrees. A single flaring event is seen from Starlink-1906 (NORAD classification C, i.e. classified) reaching a maximum of 3.09 at 109 degrees. Observations are on average ~ 2 magnitudes brighter at larger Solar phase angles, dominated by specular chassis scatter [13]. The V1.5 satellites on average also trend linearly in brightness with Solar phase angle from 110 degrees onwards. We examine trends in this region in more detail below. From 70 degrees to 110 degrees however, significant deviations from the linear trend is seen, with some satellites exhibiting substantial increases in brightness of ~ 1.5 magnitudes, while others continue a downward trend, and others reducing in brightness by ~ 1 magnitude. These contrasting light curves indicate the complexity of the scattering surface, may be due to varying Solar array configurations, and satellite designs. For example, modified Starlink satellites such as the "visor sat" [16] and satellites with various reflective and flocking surfaces designed to reduce brightness in terminator illumination conditions may have different reflective properties consistent with smaller Solar phase angles. We see a roughly flat trend with Solar phase angle for V2.0 satellites. Notably are two regions at 90 and 120 degrees where large troughs or peaks are seen in the light curves, depending on the satellite observed.

In addition to Starlink satellites, we also observe a range of larger satellites during the day successfully. These results are presented in [6] and [7].

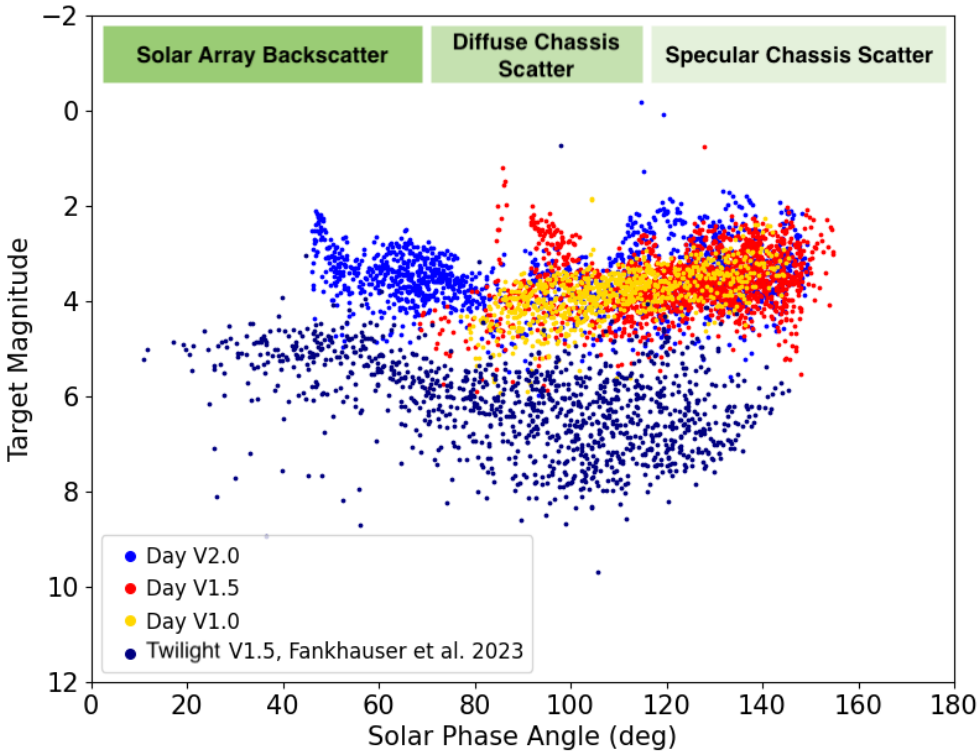

Fig. 5: Daytime observed target magnitudes for Starlink satellites in sloan r' as a function of Solar phase angle. V1.0 are shown in yellow, V1.5 in red and V2.0 in blue. Pomenis observatory twilight observations of V1.5 satellites from [13] are shown in navy, in addition to the scattering regions described in the same work in green above. We note that the relationship between Solar phase angle and target magnitude for Starlink satellites is complex, and varies between satellite versions. The median brightness is also 2.6 magnitudes brighter during the day than twilight observations. We also note a lack of observations of V1.5 and V1.0 satellites at Solar phase angles greater than ~ 60 degrees which may be due to observational or detection limit biases.

3.5 Comparison of Starlink Observations to Satellite Brightness Models

In order to explore why the Starlink satellites are ~ 11 times brighter during the day than expected, we employ the satellite optical brightness modelling package `lumos-sat` described in [13].

Using the method described in subsection 2.2, we predict the magnitude of the pass at each observation location, taking into account the different Solar panel and chassis sizes, assuming all are in a nominal operating orientation, with adjusted Solar constant to accommodate for our observation bandpass. We use the Phong BRDF parameters for the scattering function of the surface of the Earth given by [13] for the ocean, due to the fact that they spend a majority of the duration of the pass over the east coast of Australia. These are $K_d = 0.48$ for diffuse surface albedo, $K_s = 0.08$ for the magnitude of the spectacular component, and n = 16.45 for the width of the specular peak. We assume the same BRDF profile generated using in lab testing in [13] for the V1.5 satellites for all versions in this work, as we do not have access to any further information about the scattering properties of V1.0 or V2.0 satellites.

The model is run twice to calculate magnitudes with and without including an Earthshine component, and the residuals are shown as histograms in Figure 7 for each satellite version. Firstly, the mostly clumpy nature of the residuals in the sense that all versions tend to have a similar offset indicates the general assumptions about each version are approximately correct. We remind the reader that only V1.5 satellites are using an informed spacecraft design, while for the other versions we had to make assumptions about their physical properties (see section 2).

Now considering the two models, we show in Figure 7 that for the model without including Earthshine, the residuals are large for all versions of 8.26mag, $\sigma = 2.28$mag for V2.0, 7.67mag, $\sigma = 2.45$mag for V1.5 and 7.96mag, $\sigma = 1.97$mag,

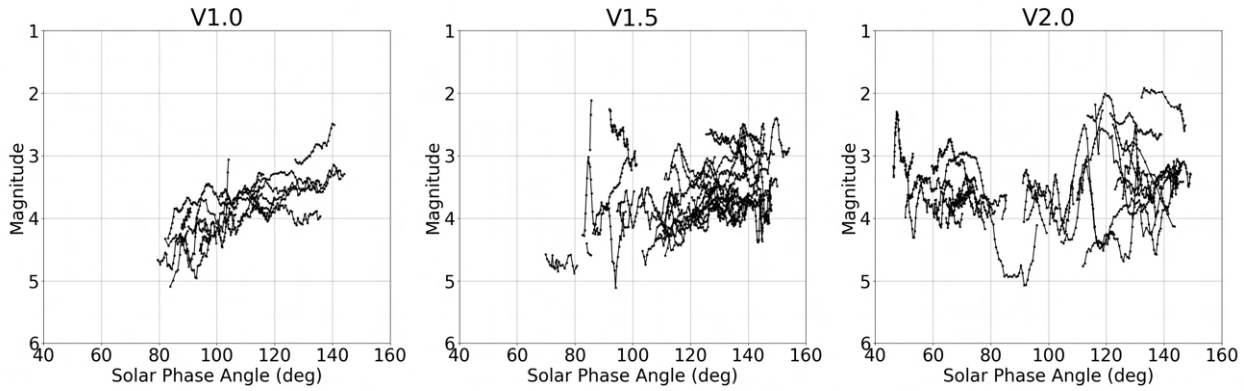

Fig. 6: Satellite observed magnitude in sloan r' as a function of Solar phase angle for all targets observed. Light curves are broken into different plot panels according to their version number. We also use rolling median with observation time to reduce the impact of seeing/scintillation noise which is significant during the day. We observe an approximately linear trend with Solar phase angle for V1.0, increasing in complexity to V2.0, possibly reflecting the increased complexity of design and operation of the satellites with later versions.

approaching an average of $\sim 2000\times$ fainter than what we observe. We also find that there are some observations that span between -10 and 0 magnitudes in residuals, indicating that there only a few passes for which Earthshine is not the dominant component of the scattered flux. For the model including Earthshine we find residuals of 0.89mag, $\sigma = 0.82$mag for V2.0, 0.4mag, $\sigma = 1.01$mag for V1.5 and 0.73mag, $\sigma = 0.37$mag for V1.0.

The difference between model predictions shown in Figure 7 indicates that light scattered off the Earth's surface is a significant factor in the brightness of satellites during the day. This is similar to the finding of [13] for observations of satellites in terminator illuminated conditions after Sunset. We find that the model best describes the brightness of V1.5 satellites, which is consistent with using the V1.5 surface BRDF (which was provided by SpaceX) for these calculations[12]. For the other satellite versions, we note again that we had to make assumptions about their physical properties. The V1.0 model is consistently brighter than the model predicts. This indicates that the scattering surface on these satellites is either more reflective than the V1.5's and requires an updated surface BRDF model, or the Solar panel array or chassis is larger than the rough estimate found online. Finally the V2.0 satellite model has the most variation from the model, and is fainter than calculated in the model. This may be due to an overestimation of the size of the Solar panel array, or improved brightness reduction surfaces. Not all V2.0 satellites may have the same solar panel array, and so may less scattering surface area than is used in this model [14]. However, SpaceX does not provide information about which satellites are in what configuration. Additionally, the scattering surface of the satellites could be less reflective than the V1.5 satellites.

To further explore possible physical differences between each version, we isolate a set of "control sample" data and present in Figure 8 light curves and transit paths of two satellites of each version. The control sample satellites have the largest number of individual observations and largest Solar phase angle range. Black data points have a mean rolling window of 7 observations, and light grey points are individual observations. The red dotted line is the predicted magnitude of the target from the model that includes Earthshine.

For the two V2.0 satellites we see similarities in the light curve with a peak at 114 degrees, followed by troughs at different Solar phase angles. The two satellites are transiting in front of the Sun in mirrored paths, but similar Sun altitudes. This may explain the variation in light curves as different sides of the chassis is visible to the observer at this phase angle. V1.5 and V1.0 do not show these statistically significant peaks and troughs. However we do note qualitatively that V1.5 satellites do appear to be more complex than V1.0.

Model light curves show similar rise or small of the data, but do not capture the complexity of the light curves. The lack of complexity in the predictions is likely due to the simplicity of the scattering surfaces modeled, which does not contain any information about self shadowing of components, differences in scattering properties on different parts of

[12]Only a single outlier satellite Starlink-5424 is found to cause a deviation in the distribution which is brighter than what the model predicts. We discuss this satellite in further detail in section 4.

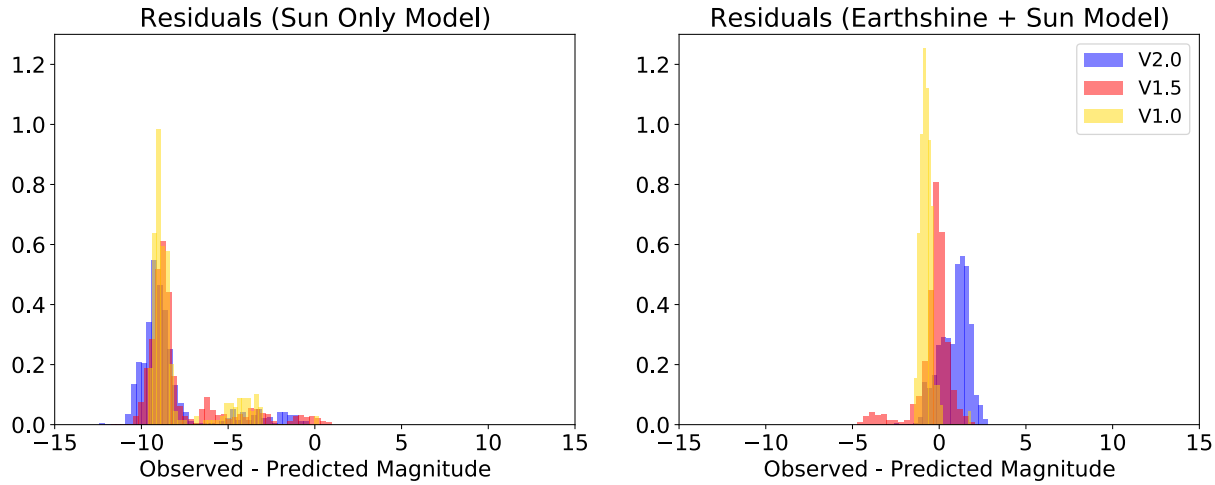

Fig. 7: Predicted sloan r' target magnitude subtracted from observed target magnitude for two model configurations. The left panel shows residuals for a model without including a light source due to Earthshine, and the right includes Earthshine. We find that the model that best fits the data is that which includes contributions due to light scattering off the surface of the Earth, in agreement with a similar conclusion for observations during terminator conditions [13]. Our work indicates the Earthshine is a significant contributors to the brightness of satellites during the day. For the model including Earthshine we find mean residuals of $0.89, \sigma = 0.82$mag for V2.0, $0.4, \sigma = 1.01$mag for V1.5 and $0.73, \sigma = 0.37$mag for V1.0. Discrepancies between observations and the model including Earthshine are likely due to a differing scattering properties (BRDF) for the satellite or the size of satellite surface areas. The model without Earthshine shows residuals that are on average $\sim 2000\times$ fainter than what is observed.

the Solar array (front vs back for example) or the chassis. We find again that V2.0 models overestimate the brightness of the target, V1.5 are a good order of magnitude fit, and V1.0 models are underestimated. Again, this reflects the need to make assumptions about V1.0 and V2.0, whereas V1.5 models were provided by SpaceX in [13].

To broadly compare the models to our observations and investigate the impact of Earthshine, we compute the all sky satellite magnitude in transit path plot using models with and without Earthshine, for the V1.5 satellites in Figure 9. As described in [13], the plot can be thought of as the sky above an observer on the ground looking up, with zenith at 90 degrees in the center of the plot, stepping down in units of 10 degrees to the horizon along the circumference of the plot. It can be used to predict where it is most likely to see a satellite during the day. Figure 9 shows that the model without Earthshine does a poor job explaining the data, particularly for large Solar phase angles. The bright spot in these plots corresponds to Sunlight specular reflection off the Solar array at small Solar phase angles, which decreases in brightness as the Sun sets. The model cannot explain the brightest observations at larger Solar phase angles, where the satellite is directly overhead from the observer.

The model that incorporates Earthshine better matches the observations. The data seem to support the idea presented in [13] that there is a bright Solar panel spot opposite the Sun at large phase angles due to Earthshine, as well as a diffuse and specular Earthshine scattering component off the chassis.

4. APPLICATIONS

There are multiple factors that impact the brightness of satellites, and contribute to their complex light curves found in this work. These may include the orientation of the satellite during the pass, it's physical size, structure and the materials that it is made of, as well as the non-uniform scattering of light off the Earth's surface [e.g., 27, 13, 26]. A possible explanation for the variations seen in Figure 6 and Figure 8 may be due to complex surface features on the body of the satellite changing the way that light is scattered from the surface, as well as the possibility of self shadowing raised by [13] and discussed in [26].

We now explore the possibility for variation that is orders of magnitude fainter or brighter than the model prediction

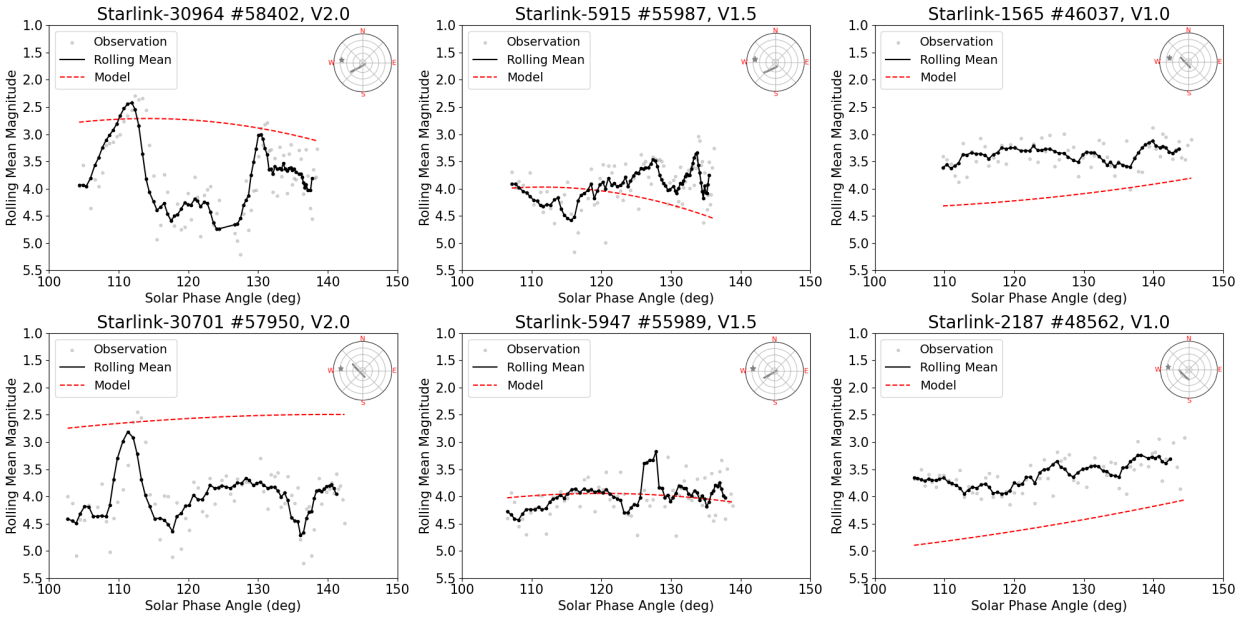

Fig. 8: "Control sample" satellite light curves for 2 of each satellite version with highest number of consecutive observations. Starlink satellite number, NORAD ID (#), and Starlink version are given in the heading. The magnitude of the target in r' band is presented as a function of Solar phase angle, in addition to the transit path in the top right hand side of each plot. Black points are rolling means (7 observations) with time to reduce the effect of seeing, with all observations plotting in light grey. The red dotted line is the predicted magnitude of the target from the model. The location of the Sun is plotted as a star, and satellite locations as grey circles in the top right transit path plot. We notice some similarities, notably a peak at $\sim$ 115 degrees phase angle, and a double trough features for the V2.0 satellites at higher Solar phase angles. The model does not capture the complexity of the light curves, but instead offers a rough order of magnitude estimate for target brightness. V2.0's are overestimates in brightness, V1.0's are under estimated, and V1.5's are the best fit, as we have information about the scattering properties and surface area from [13].

due to a satellite orbiting in an unexpected orientation (i.e. it has lost attitude control) and if these variations can be detected by the Huntsman Telescope Pathfinder during the day as a potential application of these results.

In Figure 10, we explore the impact of a change in satellite orientation with respect to the Sun, observer, and the Earth. We use an example satellite control sample, a V1.5 target, Starlink-5915, whose light curve is shown in Figure 8 and shows a similar observed magnitude as the model predictions. The flight path, and orbital altitude of the satellite is kept identical to that observed in Figure 8. We explore two scenarios, one in which the solar panel is rotated about the Z axis, such that it faces away from the Sun at various degrees away from nominal. We also explore a tumbling scenario, where the satellite is rotated about the X axis which is identified as being of interest for SpaceX SDA capabilities [11].

In the rotation scenario, the model predicts subtle variation in the light curve brightness for this particular pass that is most apparent at small Solar phase angles below 100 degrees, in the Solar array back scatter region. Variation in brightness are found to be 0.74mag, $\sigma = 0.43$mag. This change is due the variation in Solar panel surface area and therefore mostly scales by the amount of diffuse reflection as seen by the observer as the panel turns. We also see a peak at $\sim$ 140 degrees, where the satellite is closest to the Sun in its pass. This is due to a specular reflection off the Solar panel with respect to the observer and the Sun at these particular configurations.

For the tumbling scenario, the model predicts a variation in brightness of 2.7mag, $\sigma = 2.04$mag as the entire satellite is rotated. Rotations between 135 degrees and 225 degrees resulting in the satellite being fainter than the approximate Huntsman Pathfinder magnitude limit of $\sim$ 6mag (in the evening) [9] and so is not included in this plot. From these simulations we can conclude that in most scenarios, the variation in brightness from the nominal light curve is within the photometric accuracy of the Huntsman Pathfinder during the day of 0.05 ± 0.03mag [9].

While these simulations indicate that it may be possible to detect and recover changes in satellite attitude from the

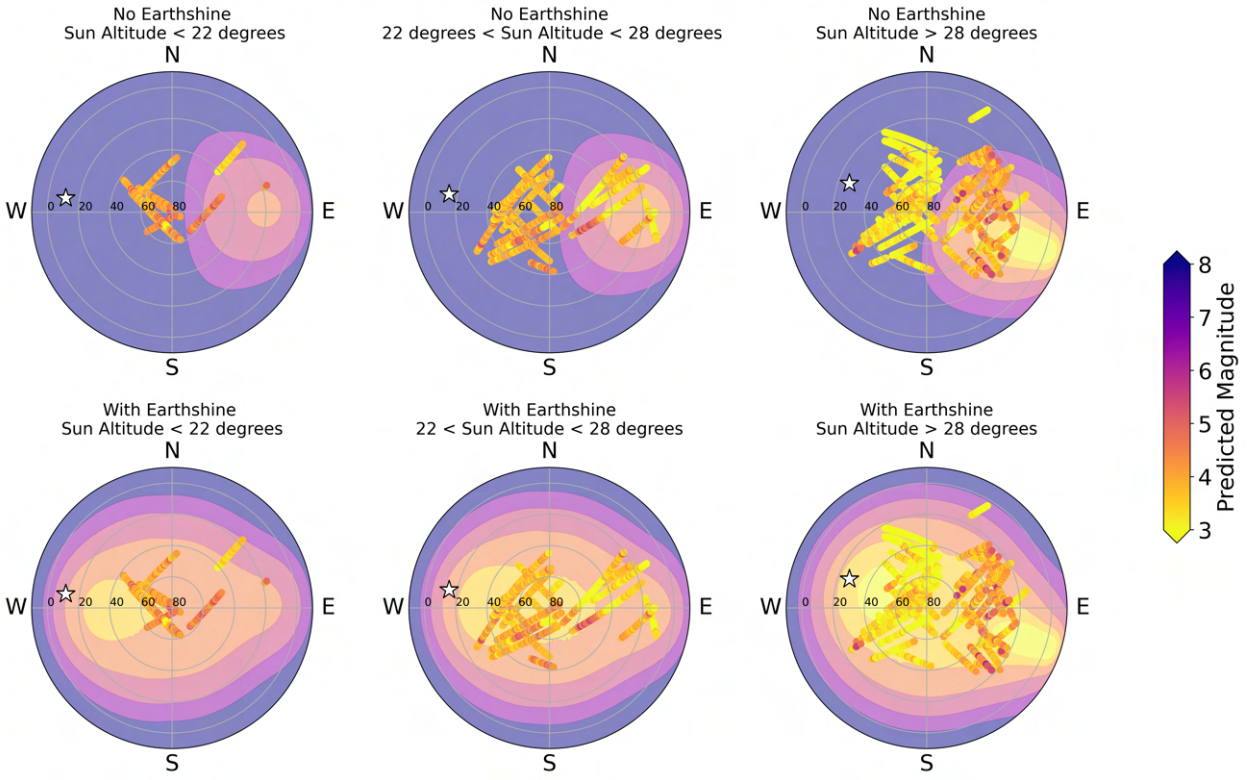

Fig. 9: Predicted V1.5 satellite magnitude across the whole sky for low, medium and high Sun altitudes, with observed V1.5 satellite brightness over plotted for all targets. The colour bar is the target magnitude. The median Sun location is shown with a white star. Zenith, or 90 degrees altitude to the perspective of an observer on the ground is the center of the plot, stepping down to the horizon in units of 10 degrees to the circumference of the plot. The top 3 panels show the predicted magnitude without Earthshine included as a light source, and the bottom 3 panels include Earthshine in the model predictions. We find that the model including Earthshine better matches the observed distribution of satellite brightness at large Solar phase angles. Starlink-5424 is shown on the far right plots as an outlier (top right quadrant), and is addressed separately below.

ground without the need for resolving the target, in order to confirm if this approach is useful, more data of similar types of satellites in similar pass configurations would be needed. These results may also be one explanation for the outlier light curve of Starlink-5424 which is observed to be brighter than predicted (see [7] and [6] for a more detailed analysis).

Due to the rise of satellite-to-satellite in orbit non-Earth imaging (NEI) imaging being explored by companies like HEO Space[13], it may be possible to map the satellite attitude to the light curve through the use of simultaneous observations. Another important factor is information to determine variations in the satellite design and scattering properties that could be incorporated into the model that would need to be provided by SpaceX. Without this further information, we are unable to decouple these findings from the remaining unknowns.

5. CONCLUSION

In conclusion, we find that Starlink satellites are visible during the day using the Huntsman Pathfinder system. By comparing results to satellite optical brightness models, we find that the surprising increase in satellite brightness of up to $\sim 11\times$ during the day as compared to twilight observations is likely due to the contribution of Earthshine below the satellite during the day.

[13]https://www.heospace.com/

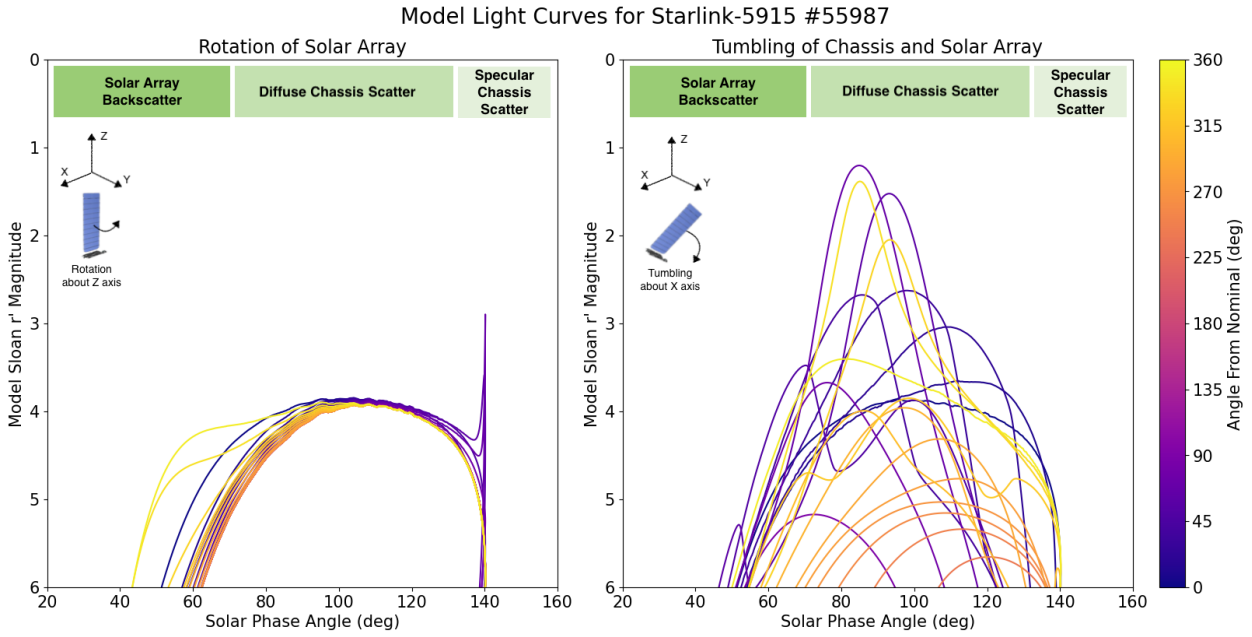

Fig. 10: We explore the impact of rotating a satellite on the predicted light curve as a function of solar phase angle for various deviations from nominal. The panel on the right shows the results of a tumbling simulation about the X axis for Starlink-5915, following the same path as shown in Figure 8. The Y axis is cut at 6 magnitudes which is a reasonable detection limit for the Huntsman Pathfinder in optimal daytime observing conditions. Passes between 135 and 225 degrees result in light curves fainter than 6 magnitudes and so are not shown. Scattering regions are shown in green above for reference. Large deviations in brightness from the nominal configuration are seen with a mean of 2.7mag, $\sigma = 2.04$mag , which may be easily detected by the Huntsman Pathfinder system. The panel on the left shows a scenario for a rotating solar panel, which keeps the chassis pointing toward the Earth in a nominal configuration and resulting in a mean variation of 0.74mag, $\sigma = 0.43$mag is seen. These results indicate it may be possible to determine the orientation of a satellite in orbit from the light curve using the Huntsman Pathfinder.

The key results of this work include:

- Starlink satellites (V1.0, V1.5 and V2.0) are found to have a median brightness of 3.6mag, $\sigma = 0.6$mag in sloan r' during the day.
- By comparing observations to theoretical models, we conclude that this surprising brightness can be explained by the contribution of Earthshine scattered off the surface of the Earth beneath the telescope during daytime passes.
- We find that Starlink satellites have on average become progressively brighter during the day with newer versions.
- We present light curves for 81 Starlink satellites, and conclude that these light curves are more complex than theoretical models, and show some similarities between satellite versions.
- Using simulated satellite daytime light curves, we conclude that it may be possible to detect changes in satellite orientation with the Huntsman Telescope system based on changes in the light curve of the satellite without resolving the target during the day.

These findings demonstrate the potential for small optical telescopes built predominately from off the self hardware to make a meaningful contributing to Space Domain Awareness efforts during the day. This is particularly useful in the upcoming era of mega constellation such as AST's Space Mobile (BlueWalker 3), Eutelsat's OneWeb, Amazon's

Project Kuiper, and Starlink. With the exponential growth of Starlink satellites in orbit in recent years and the planned launch of many more - particularly as we are enter the Starship generation - the ability to monitor and produce photometric light curves of starlink satellites during the day is highly desirable. This capability has the potential to make the Huntsman Telescope a highly productive SDA facility. Daytime SDA capabilities of LEO satellites will reduce the dependence on the short observation windows during terminator illuminated conditions, allowing for improvements in satellite tracking and attitude monitoring, situational awareness and object classification.

ACKNOWLEDGMENTS

The authors would like to thank and acknowledged the assistance of Forrest Fankhauser, for his continued support of this work, and for providing insights and direction in the use of *lumos-sat*.

We would like to thank Canon Australia for their support of the Huntsman Telescope collaboration and Pathfinder Huntsman project.

The authors would like to acknowledge the generous assistance of Macquarie Observatory manager Adam Joyce who has provided continued technical support of this project that has made these results possible. We would also like to thank astro-imaging guru Jack Gow from Bintel for his continued support of this work and of the Huntsman Telescope project. We would also like to acknowledge the ever present, enthusiastic support of friends from the Association For Astronomy (AFA), Macquarie University.

Finally the authors would like to acknowledge the traditional owners of the land on which the Huntsman Telescope is situated, Gamilarray, Wiradjuri and Wayilwan Country. In addition we would like to acknowledged the traditional owners of the land on which the Macquarie University Observatory is located, the Wallumattagal Clan of the Dharug Nation – whose cultures and customs have nurtured, and continue to nurture, this land since time immemorial.

Software: Lumos-sat (Fankhauser, F. et al. 2023) Astropy (The Astropy Collaboration 2013, 2018), Scipy (Virtanen, P. et al, 2020), Photutils (Bradley, L. et al, 2016), Source Extractor (Bertin, E. et al, 1996), Skyfield (Rhodes, B. et al, 2019),

Author Contribution Statement:
Sarah E. Caddy: Conceptualization, Methodology, Software, Formal analysis, Investigation, Writing, Editing.
Lee R. Spitler: Supervision, Conceptualization, Review & Editing.

Funding Statement: S.C. and L.S. acknowledge support from an Australian Research Council Discovery Project grant DP190102448

Competing Interests: The authors report no conflict of interest to the best of our knowledge at the time of publication.

Data Availability Statement: Data collected with the Huntsman Pathfinder for the purposes of this work, and the python code used to reduce the data may be made available at the request of the first author.

REFERENCES

[1] Miguel R. Alarcon, Javier Licandro, Miquel Serra-Ricart, Enrique Joven, Vicens Gaitan, and Rebeca de Sousa. Scientific CMOS Sensors in Astronomy: IMX455 and IMX411. *Publications of the Astronomical Society of the Pacific*, 135(1047):055001, May 2023. Publisher: The Astronomical Society of the Pacific.

[2] Antonella A. Albuja, Daniel J. Scheeres, and Jay W. McMahon. Evolution of angular velocity for defunct satellites as a result of YORP: An initial study. *Advances in Space Research*, 56(2):237–251, July 2015.

[3] Australian Department of Defence. 2020 Force Structure Plan, 2020. ISBN: 978-0-9941680-6-1.

[4] Christopher R Binz, Mark A Davis, Bernie E Kelm, and Christopher I Moore. Optical Survey of the Tumble Rates of Retired GEO Satellites. September 2014.

[5] Laurence David James Blacketer. *Attitude Characterisation of Space Objects using Optical Light Curves*. PhD thesis, University of Southampton, March 2022.

[6] Sarah E. Caddy. Astronomical ideas to innovation. Thesis under review, Macquarie University, 2024.

[7] Sarah E. Caddy and Lee R. Spitler. Daytime photometry of starlink satellites with the huntsman telescope pathfinder. *The Journal of the Astronautical Sciences*, 2024. Under review.

[8] Sarah E. Caddy, Lee R. Spitler, and Simon C. Ellis. Toward a Data-driven Model of the Sky from Low Earth Orbit as Observed by the Hubble Space Telescope. *The Astronomical Journal*, 164(2):52, July 2022. Publisher: The American Astronomical Society.

[9] Sarah E. Caddy, Lee R. Spitler, and Simon C. Ellis. An optical daytime astronomy pathfinder for the huntsman telescope. *PASA*, 164(2):52, July 2024. Publisher: The American Astronomical Society.

[10] Paul Chote, James A Blake, and Don Pollacco. Precision Optical Light Curves of LEO and GEO Objects. 2019.

[11] Richard DalBello. Re: SpaceX Comment-Office of Space Commerce, National Oceanic and Atmospheric Administration, Department of Commerce, Request for Information (RFI) on Scope of Civil Space Situational Awareness Services (88 FR 4970), February 2023.

[12] Nathan Estell, Dylan Ma, and Patrick Seitzer. Daylight Imaging of LEO Satellites Using COTS Hardware. In *Advanced Maui Optical and Space Surveillance Technologies Conference*, September 2019. Conference Name: Advanced Maui Optical and Space Surveillance Technologies Conference Pages: 26 ADS Bibcode: 2019amos.confE..26E.

[13] Forrest Fankhauser, J. Anthony Tyson, and Jacob Askari. Satellite Optical Brightness. *The Astronomical Journal*, 166(2):59, July 2023. Publisher: The American Astronomical Society.

[14] David Goldman. IBFS File Nos. SAT-LOA-20200526-00055 and SAT-AMD-20210818-00105, August 2022.

[15] Alan W. Greynolds. General physically-realistic BRDF models for computing stray light from arbitrary isotropic surfaces. In *Optical Modeling and Performance Predictions VII*, volume 9577, pages 97–104, San Diego, California, USA, September 2015. SPIE.

[16] Takashi Horiuchi, Hidekazu Hanayama, Masatoshi Ohishi, Tatsuya Nakaoka, Ryo Imazawa, Koji S Kawabata, Jun Takahashi, Hiroki Onozato, Tomoki Saito, Masayuki Yamanaka, Daisaku Nogami, Yusuke Tampo, Naoto Kojiguchi, Jumpei Ito, Masaaki Shibata, Malte Schramm, Yumiko Oasa, Takahiro Kanai, Kohei Oide, Katsuhiro L Murata, Ryohei Hosokawa, Yutaka Takamatsu, Yuri Imai, Naohiro Ito, Masafumi Niwano, Seiko Takagi, Tatsuharu Ono, and Vladimir V Kouprianov. Multicolor and multi-spot observations of Starlink's Visorsat. *Publications of the Astronomical Society of Japan*, 75(3):584–606, June 2023.

[17] Anthony Horton, Lee Spitler, Wilfred Gee, Fergus Longbottom, Jaime Alvarado-Montes, Amir Bazkiaei, Sarah Caddy, and Steven Lee. The Huntsman Telescope: lessons learned from building an autonomous telescope from COTS components. In *Advances in Optical Astronomical Instrumentation 2019*, volume 11203, pages 5–6. SPIE, January 2020.

[18] Sunita Jahirabadkar, Prajakta Narsay, Shivani Pharande, Gargi Deshpande, and Anusha Kitture. Space objects classification techniques: A survey. In *2020 International Conference on Computational Performance Evaluation (ComPE)*, pages 786–791, 2020.

[19] Krzysztof Kamiński, Michał Żołnowski, Monika K. Kamińska, Mikołaj Krużyński, Dorota Krużyńska, and Edwin Wnuk. Optimizing visual daytime satellite observations. 2021.

[20] Emma Kerr, Gabriele Falco, Nina Maric, David Petit, Patrick Talon, Elisabeth Geistere Petersen, Chris Dorn, Stuart Eves, Noelia Sánchez-Ortiz, Raul Dominguez Gonzalez, and Jaime Nomen-Torres. Light curves for geo object characterization. Darmstadt, Germany, April 2021. ESA Space Debris Office.

[21] N Koshkin, L Shakun, O Kozhukhov, D Kozhukhov, V Mamarev, V Prysiaznyi, A Ozeryan, V Kudak, and I Neubauer. Simultaneous multi-site photometry or leo satellites for rotation characterization. Darmstadt, Germany, April 2021. ESA Space Debris Office.

[22] Bhavya Lal, Asha Balakrishnan, Becaja Caldwell, Reina Buenconsejo, and Sara Carioscia. Global Trends in Space Situational Awareness and Space Traffic Management, April 2018.

[23] Lorenzo Mariani, Lorenzo Cimino, Matteo Rossetti, Mascia Bucciarelli, Shariar Hadji Hossein, Simone Varanese, Gaetano Zarcone, Marco Castronuovo, Alessandra Di Cecco, Paolo Marzioli, and Fabrizio Piergentili. A Dual Perspective on Geostationary Satellite Monitoring Using DSLR RGB and sCMOS Sloan Filters. *Aerospace*, 10(12):1026, December 2023. Number: 12 Publisher: Multidisciplinary Digital Publishing Institute.

[24] Yuri Matsushita, Ryohei Arakawa, Yasuhiro Yoshimura, and Toshiya Hanada. Light Curve Analysis and Attitude Estimation of Space Objects Focusing on Glint. In *First Int'l. Orbital Debris Conf*, 2019.

[25] P. Papushev, Yu. Karavaev, and M. Mishina. Investigations of the evolution of optical characteristics and dynamics of proper rotation of uncontrolled geostationary artificial satellites. *Advances in Space Research*, 43(9):1416–1422, May 2009.

[26] Fabrizio Piergentili, Gaetano Zarcone, Leonardo Parisi, Lorenzo Mariani, Shariar Hadji Hossein, and Fabio Santoni. LEO Object's Light-Curve Acquisition System and Their Inversion for Attitude Reconstruction. *Aerospace*, 8(1):4, January 2021. Number: 1 Publisher: Multidisciplinary Digital Publishing Institute.

[27] Randa Qashoa and Regina Lee. Classification of Low Earth Orbit (LEO) Resident Space Objects' (RSO) Light Curves Using a Support Vector Machine (SVM) and Long Short-Term Memory (LSTM). *Sensors (Basel, Switzerland)*, 23(14):6539, July 2023.

[28] Brandon Rhodes. Skyfield: High precision research-grade positions for planets and Earth satellites generator. *Astrophysics Source Code Library*, page ascl:1907.024, July 2019. ADS Bibcode: 2019ascl.soft07024R.

[29] M. Roggemann, D. Douglas, E. Therkildsen, D. Archambeault, R. Maeda, D. Schultz, and B. Wheeler. Daytime Image Measurement and Reconstruction for Space Situational Awareness Applications. Wailea, Maui, Hawaii, September 2010. Advanced Maui Optical and Space Surveillance Technologies Conference. Conference Name: Advanced Maui Optical and Space Surveillance Technologies Conference Pages: E17 ADS Bibcode: 2010amos.confE..17R.

[30] E. W. Rork, S. S. Lin, and A. J. Yakutis. Ground-based electro-optical detection of artificial satellites in daylight from reflected sunlight. *NASA STI/Recon Technical Report N*, 83:10098, May 1982. ADS Bibcode: 1982STIN...8310098R.

[31] Jeff Shaddix, Jacob Brannum, Alex Ferris, Austin Hariri, Ari Larson, Tyler Mancini, and Jeff Aristoff. Daytime GEO Tracking with "Aquila": Approach and Results from a New Ground-Based SWIR Small Telescope System. Maui, Hawaii, USA, 2019. Advanced Maui Optical and Space Surveillance Technologies Conference.

[32] Jeff Shaddix, Cameron Key, Alex Ferris, James Herring, Navraj Singh, Todd Brost, and Jeff Aristoff. Daytime Optical Contributions Toward Timely Space Domain Awareness in Low Earth Orbit. Maui, Hawaii, USA, 2021. Advanced Maui Optical and Space Surveillance Technologies Conference.

[33] J. Silha, T. Schildknecht, J. Pittet, D. Bodenmann, R. Kanzler, P. Karrang, and H. Krag. Comparison of ENVISAT's Attitude Simulation and Real Optical and SLR Observations in order to Refine the Satellite Attitude Model. In *Proceedings of the Advanced Maui Optical and Space Surveillance Technologies Conference*, September 2016. Conference Name: Advanced Maui Optical and Space Surveillance Technologies Conference Pages: 54 ADS Bibcode: 2016amos.confE..54S.

[34] Jiří Silha, Jean-Noël Pittet, Michal Hamara, and Thomas Schildknecht. Apparent rotation properties of space debris extracted from photometric measurements. *Advances in Space Research*, 61(3):844–861, February 2018.

[35] Jovan Skuljan. Photometric measurements of geostationary satellites over the Western Pacific Region. Maui, Hawaii, USA, 2018. Advanced Maui Optical and Space Surveillance Technologies Conference.

[36] The Astropy Collaboration. The Astropy Project: Sustaining and Growing a Community-oriented Open-source Project and the Latest Major Release (v5.0) of the Core Package*. *The Astrophysical Journal*, 935(2):167, August 2022. Publisher: The American Astronomical Society.

[37] United Nations Office for Outer Space Affairs. *Guidelines for the Long-term Sustainability of Outer Space Activities of the Committee on the Peaceful Uses of Outer Space*. United Nations, Vienna, Austria, January 2021.

[38] United States Space Force. Space Domain Awareness: Doctrine for Space Forces, November 2023.

[39] Peter Zimmer, Mark Ackermann, and John McGraw. Optimizing Daylight Performance of Small Visible-NIR Optical Systems. Maui, Hawaii, USA, 2020. Advanced Maui Optical and Space Surveillance Technologies Conference.

[40] Peter Zimmer, John McGraw, and Mark Ackermann. Overcoming the Challenges of Daylight Optical Tracking of LEOs. Maui, Hawaii, USA, 2021. Advanced Maui Optical and Space Surveillance Technologies Conference.